

---

---

# A Very Large Eddy Simulation Model Using a Reductionist Inlet Turbulence Generator and Wall Modeling for Stable Atmospheric Boundary Layers

M. Ahmadi-Baloutaki<sup>a,\*</sup> and A. A. Aliabadi<sup>a,\*\*</sup>

<sup>a</sup> Atmospheric Innovations Research (AIR) Laboratory, Environmental Engineering, School of Engineering, RICH 2515,  
University of Guelph, Guelph, ON, N1G 2W1, Canada

\*e-mail: mahmadib@uoguelph.ca

\*\*e-mail: aliabadi@uoguelph.ca

Received April 28, 2020; revised September 20, 2020; accepted October 20, 2020

**Abstract**—Despite many advances in numerical simulation of stable boundary layers (SBL), most of the models developed are complex and computationally expensive. A computational fluid dynamics (CFD) strategy is proposed that combines very large eddy simulation (VLES) with a reductionist inflow turbulence generator and wall modeling aimed at affordable and practical simulation of SBL. Unlike the standard LES requiring the filter width to be of the scale of grid size, the filter width in VLES can be set at a value between the grid size and the large characteristic length scales of the flow. This strategy, along with the application of wall treatments, results in the significant reduction of computational costs. Moreover, the reductionist approach of the inflow turbulence generator minimizes the number of required input parameters to the model, which makes the model suitable for practical applications. A series of sensitivity studies are conducted to refine the numerical parameters including the grid resolution, filter width, and the inflow turbulence generator variables controlling the length and time scales of the eddies generated at the inlet. The performance of the model is successfully evaluated against wind-tunnel measurements for mean velocity, mean temperature, and turbulence profiles for four different thermal stability levels ranging from weak to strong stability. The spectral analysis of the model for velocity components, temperature, momentum, and heat fluxes showed that the model is capable of successfully resolving the energy cascade for almost two orders of magnitude of wave numbers and partially matching the well-known log-log slopes for the inertial subrange.

**Keywords:** inlet turbulence generation, stable boundary layer, very large eddy simulation, wall modeling

**DOI:** 10.1134/S0015462821020026

## 1. INTRODUCTION

A thermally stratified boundary layer is a common atmospheric condition found in nocturnal and cold climate atmospheric boundary layers (ABL), where the ground is colder than the air. In such boundary layers, the buoyancy forces caused by thermal stratification have a stabilizing effect on the boundary layer by suppressing turbulent transport especially in the vertical direction [1]. The damping of turbulent motions by thermal stratification in stably stratified or stable boundary layers (SBL) results in generally low turbulence levels along with small-scale eddies populating the boundary layer [2]. The flow properties within the SBL vary with the level of thermal stratification or stability strength. A universal parameter to specify the strength of the thermal stratification level is the Richardson number, which is the ratio of buoyant production to turbulence shear production in the turbulence kinetic energy (TKE) budget equation [3, 4] to be defined later.

There have been many modeling efforts to understand the turbulence structure of ABL using various numerical techniques. While direct numerical simulations (DNS) are too computationally expensive and Reynolds-averaged Navier–Stokes (RANS) or eddy viscosity models suffer from lack of accuracy, large eddy simulations (LES) have been used as an effective numerical tool to simulate the ABL with sufficient reliability [5]. In LES, the turbulent eddies of the size of the computational grid cells and larger are explicitly resolved, while the effects of the smaller eddies are parameterized using subgrid scale (SGS) models [6].

Although there has been many progress in LES of ABLs, the general success of LES models for a particular application is not guaranteed. Most of the successful LES studies of ABLs have been conducted on convective boundary layers (CBL), which have large energy containing eddies in the order of the size of the boundary layer height [7, 8]. The success of these LES models is mainly attributed to the dominance of the large-scale structures in the CBL flows [7]. On the other hand, LES of stable boundary layers requires higher grid resolutions and more accurate SGS models to simulate the relatively small boundary layer turbulence scales reasonably well [2]. Moreover, the accuracy of LES models may be limited by the lack of realistic perturbation fields in their inlet boundary conditions, grid resolution, and subsequently non-resolved turbulence scales down to the finest scales of the inertial subrange and near the walls [9]. These challenges and the methods addressing them will be briefly reviewed in the following sections.

### *1.1. Inlet Turbulence*

In order to build a robust LES model for simulating the turbulent ABL realistic turbulent fluctuations need to be introduced at the inlet that would evolve in the entire domain. From the theoretical stand point, the fluctuations must meet several criteria: (a) they must be stochastically varying on scales down to the spatial and temporal filter scales; (b) they must be compatible with the Navier—Stokes equations; (c) they must be composed of coherent eddies across a range of spatial scales down to the filter length; (d) they must allow easy specification of turbulence properties; and (e) they must be easy to implement [10].

Two of the most common approaches to generate the inlet turbulent fluctuations for LES models are the synthetic and precursor methods. In the synthetic method, random fields are constructed at the inlet, while in the precursor method an additional simulation is performed to generate the desired fluctuations. The precursor methods are shown to be more accurate but more computationally demanding and more difficult to implement [10]. These methods have been reviewed in the literature [10] and are not discussed in the rest of this paper. The synthetic method, which is the method of choice to generate the inflow turbulence in the present work, is briefly discussed here. A more detailed review of synthetic methods can be found in [9, 10].

Lund et al. [11] developed a synthetic model, originally introduced by Spalart [12], to generate the inlet turbulent fluctuations by rescaling the velocity field at a downstream station, and re-introducing it as a boundary condition at the inlet, and hence developing spatial and temporal turbulent boundary layers economically. Compared to primitive methods of random inclusion of perturbations at inlet, it has been shown that this synthetic method reduces adaptation distance downstream of the flow down to ten times the boundary-layer height [11]. Another common synthetic model is the vortex method originally developed by Sergent [13] and later refined in [14–16]; it inserts random two-dimensional vortices at the inlet boundary that evolve in the simulation domain. These vortices are parameterized by realistic length scales, times scales, and vorticity magnitudes, formulated from mean flow information and grid spacing. Abo-shosha et al. [17] developed a method based on synthesizing random divergence-free turbulence velocities with consideration of spectra and coherency functions that match the ABL flow statistics. This scheme maintains both the turbulence spectrum and coherency function.

The synthetic vortex method is chosen to generate the inlet turbulence in the current simulations, in view of its robust performance and reductionist approach. Compared to other methods, the synthetic vortex method only requires a handful of parameters to generate a realistic turbulent flow field at the inlet section and consequently in the entire domain.

### *1.2. Grid Resolution*

Due to the presence of small-scale eddies within the SBL, low grid resolutions have been associated with the problems encountered in some LES works [2, 6]. Beare and Macvean [18] conducted a series of large-eddy simulations of the SBL with a wide range of mesh sizes and found that both mean and turbulent variables depend strongly on the mesh size even for obtaining converged solutions. In another LES study of the SBL, de Roode et al. [19] used isotropic grids with varying mesh sizes and found that the SGS TKE is significantly sensitive to the grid size. For coarse grids, the numerical domain was dominated by SGS fluxes with very small to no resolved TKE. De Roode et al. [19] reported that increasing the grid resolution limited the dominance of SGS fluxes to a very thin layer near the wall while the turbulent eddies were resolved successfully in the rest of the domain. Increasing the boundary layer stability level will require even finer levels of grid resolution and more computational power since the dominant eddies become smaller and have a more intermittent nature [18].

### 1.3. Subgrid Scale Model

The most widely used SGS model is the eddy-viscosity closure model developed by Smagorinsky [20]. In this model, the momentum transport by the unresolved velocity field is parameterized by an effective viscosity [5]. Many successful LES works for neutral and convective ABLs have used the Smagorinsky SGS model [11, 14]. The other SGS models include the Wall-Adapted Local Eddy-viscosity (WALE) model used by various investigators [21] and the one-equation SGS TKE model that has gained popularity recently [22, 23].

For the SBL, however, there have been some efforts on investigating the potential influence of the boundary layer stability on the Smagorinsky model's performance. Using a Smagorinsky model with wall damping and stability correction functions, Mason and Derbyshire [24] conducted large-eddy simulations of the SBL and attributed failures in the simulations to the SGS model and excessive grid resolutions forced by the limitation of computational resources. Saiki et al. [25] used a modified two-part SGS model in their LES modeling of the SBL and reported numerical instabilities originating from the numerics and the SGS model. Kleissl et al. [26] compared the performance of two SGS models, a scale-invariant and a scale-dependent, in the large-eddy simulations of the SBL and examined the dependence of these models on the stability and height above the ground. They concluded that the scale-dependent model gives accurate predictions of the stability-corrected Smagorinsky coefficient, while the scale-invariant one underestimates this coefficient. In a more comprehensive LES study, Bou-Zeid et al. [27] studied the effect of SGS fluxes and dissipations on small scale turbulence in the stable boundary layer using a specifically designed field experiment. They found that the stability does not alter the fraction of SGS fluxes over the total, while the SGS model coefficients vary considerably with stability. Despite these efforts, there have been many successful large-eddy simulations of SBL using the simple Smagorinsky SGS model [18, 19, 28].

### 1.4. Wall Modeling

In order to economize the computational fluid dynamics (CFD) simulations, wall functions have been largely used to model the near-wall regions basing on the hypothesis of wall similarity for both smooth- and rough-wall boundary layers in the outer layer [9]. For simulation of the atmospheric boundary layer, it is common to use a wall function based on the aerodynamics roughness length scale  $z_0$  [29]. Wall functions generally predict a log-law, i.e., the linear relationship between  $U^+ = U/u_\tau$  and logarithm of  $z^+ = zu_\tau/\nu$ , where  $u_\tau$  is friction velocity and  $\nu$  is kinematic viscosity.

Similarly to the velocity wall functions, the temperature wall functions have also been widely used to reduce the computational cost of the CFD models. The most commonly used temperature wall function for the CFD simulations is based on the similarity of momentum and heat transfer fields described in [30]. There have been some refinements for temperature wall functions for different thermal stability regimes. Using asymptotic blending of natural and forced convection Balaji et al. [31] developed wall functions for the flow inside vertical parallel plate channels suitable for mixed convection that can be used for all values of the Richardson number. Defraeye et al. [32] also developed a temperature wall function valid for both natural and forced convection flows as a parameter of the Richardson number for the ABL over wall-mounted bluff bodies. They reported more accurate results from their CFD solver using this temperature wall function compared to the case with forced-convection wall function. Along with these developments, there have been many successful LES works, e.g. in [23, 33], over the atmospheric boundary layer at different thermal stratification levels that used the classic thermal wall function described in [30].

### 1.5. Hybrid LES Methods and VLES

Due to the high computational costs of LES models, especially for the simulations of large domains common in meteorological applications, hybrid LES methods were developed to reduce the computational costs while maintaining the accuracy. Although many hybrid methods have been proposed in the literature, their naming convention and categorization is still ambiguous and interchangeable. Nevertheless, the most common group of hybrid CFD methods is known as hybrid RANS-LES that employs RANS model within a portion of the domain [34]. These hybrid RANS-LES models are categorized into two major classes of zonal and non-zonal approaches based on the strategy utilized for defining the border between RANS and LES domains [35]. In zonal methods, the computational domain is divided into two zones by a separating border defined as a series of fixed geometrical surfaces. The RANS and LES simulations are then conducted in each corresponding zone before matching the two solutions. The major drawback of this method is the requirement for complex coupling conditions at the separating border [36]. In the non-zonal approach, the RANS-LES border is established by the formulations of customized border conditions. For instance, in a non-zonal method like detached-eddy simulation (DES), the RANS is

applied to the whole or a major part of the attached boundary layer, while the separated flow regions are simulated by LES [37]. The non-zonal approach is more straightforward to set up and there have been many improvements to increase their accuracy. In a group of non-zonal methods called wall-modeling in LES (WMLES), the contribution of RANS is limited to a very thin region near walls. This approach is used in the current study.

In addition to the numerical techniques used in hybrid LES methods, VLES is another powerful tool to economize the CFD simulations. The concept of VLES originally proposed by Speziale [38] is one of the earliest hybrid CFD methods. The main distinction between VLES and the standard LES is the determination of filter width with respect to the grid size. In the pure LES, the filter width is associated with the grid size, while the filter width in VLES can be set arbitrarily at any value between the grid size and the large characteristic length scales of the flow [35, 37]. Increasing the filter width will reduce the simulation accuracy [35, 39]. This can be attributed to the fact that the greater filter width reduces the ratio of resolved-to-modeled eddies in VLES. The effect of increasing the filter width on the computational cost of the model is unclear since in VLES the filter width could be varied without changing the grid size. Based on this definition, the VLES becomes LES, when the filter width is set as its lowest limit of grid size. Pope [40] proposed a numerical definition for the distinction between LES and VLES. According to Pope [40], a LES with sufficiently fine grid and filter length should resolve more than 80% of the TKE everywhere in the domain, except near-wall regions, when wall treatments are used. In contrast, the VLES is defined as a model with coarse grid size and filter length that would resolve less than 80% of the TKE in the domain. The fractions of resolved and modeled TKE are calculated and reported in the present work to provide insights in the numerical performance of the model.

### 1.6. Scope and Objectives

This study aims at adapting the VLES model for investigating stably-stratified ABLs in the practical applications. This model uses a reductionist inlet turbulence generation technique and is coupled to velocity/temperature wall functions to reduce the computational cost. The current model benefits from a careful simulation setup, a series of systematic sensitivity studies, and evaluations against wind-tunnel experiments. These components have collectively resulted in a reductionist model suitable for industrial applications where it is impractical to perform sophisticated high-resolution simulations. Additionally, the systematic sensitivity studies conducted for the SBL in this study will assist future researchers in their VLES development efforts.

The road map of this paper is as follows: an overview of the VLES code is given in Section 2. This section discusses the details of three main components of the VLES code, namely, the SGS model, the synthetic vortex method, and the wall functions. The specifics of the numerical schemes and methodologies of the VLES code are discussed in Section 3 and the model's results are presented and discussed in Section 4. Finally, a summary of the findings and some recommendations for future work are given.

## 2. DESCRIPTION OF THE VLES CODE AND THE GOVERNING EQUATIONS

The current VLES model was developed in the open source CFD software Open source Field Operation And Manipulation (OpenFOAM), version 4.0. The standard solver adapted is buoyantBoussinesqPimpleFoam, which is enabled with the oneEqEddy SGS turbulence model [41]. The LES equations for a dry and non-isothermal ABL over a flat bottom boundary are well documented in the literature [19, 22, 23]. Therefore, this section presents only a summary of these equations.

### 2.1. Formulation and Implementation of SGS Model

An incompressible turbulent flow with thermal variations based on a one-equation SGS model is considered. These assumptions result in a series of four governing equations for dimensionless variables,  $U_i$ ,  $\Theta$ , and  $k_{SGS}$ , for the present VLES model. These equations include: (1) the continuity equation, (2) the momentum transport equation, (3) the heat transport or energy equation, and (4) the SGS turbulence kinetic energy equation. These four equations are given below (Eqs. (2.1) to (2.4)) in the dimensionless form using the boundary-layer height  $\delta$  as the reference length scale, the reference upstream velocity  $U_0$ , and the reference upstream temperature  $T_0$

$$\frac{\partial \bar{U}_i}{\partial x_i} = 0, \quad (2.1)$$

$$\frac{\partial \bar{U}_i}{\partial t} + \frac{\partial}{\partial x_j} \bar{U}_i \bar{U}_j = -\frac{\partial \bar{p}}{\partial x_i} - \frac{\partial \tau_{ij}}{\partial x_j} + \frac{1}{\text{Re}} \frac{\partial^2 \bar{U}_i}{\partial x_j \partial x_j} + \text{Ri} \delta_{i3}, \quad (2.2)$$

$$\frac{\partial \bar{\Theta}}{\partial t} + \frac{\partial}{\partial x_i} \bar{U}_i \bar{\Theta} = -\frac{\partial \pi_i}{\partial x_i} + \frac{1}{\text{RePr}} \frac{\partial^2 \bar{\Theta}}{\partial x_i \partial x_i}, \quad (2.3)$$

$$\frac{\partial k_{\text{SGS}}}{\partial t} + \bar{U}_i \frac{\partial k_{\text{SGS}}}{\partial x_i} = P + B - \varepsilon + \frac{\partial}{\partial x_i} \left( \frac{2}{\text{Re}_T} \frac{\partial k_{\text{SGS}}}{\partial x_i} \right). \quad (2.4)$$

Even though all the terms in these equations are explained in detail in other works [19, 22, 23], all the terms are described briefly here. The overbar notation indicates the spatially-resolved solution for a variable;  $\bar{p} = \bar{p}^* + \frac{1}{3} \tau_{ii}$  is the resolved-scale modified kinematic pressure normalized by constant density, where  $\bar{p}^*$  is the resolved-scale static pressure;  $k_{\text{SGS}}$  is the SGS TKE;  $\tau_{ij} = \overline{U_i U_j} - \bar{U}_i \bar{U}_j = -2\nu_T \bar{S}_{ij}$  is the SGS momentum flux, where  $\bar{S}_{ij} = \left( \frac{\partial \bar{U}_i}{\partial x_j} + \frac{\partial \bar{U}_j}{\partial x_i} \right)$  is the rate of strain;  $\pi_i = \overline{U_i \Theta} - \bar{U}_i \bar{\Theta} = -v_\theta \frac{\partial \bar{\Theta}}{\partial x_i}$  is the SGS kinematic heat flux;  $\text{Re} = U_0 \delta / \nu$  is the Reynolds number,  $\text{Re}_T = U_0 \delta / \nu_T$  is the SGS model turbulence Reynolds number,  $\text{Pr} = \nu / \alpha$  is the laminar Prandtl number, and  $\text{Ri} = g \delta \Delta \Theta / (\overline{\Theta} U_0^2)$  is the Richardson number;  $P = -\tau_{ij} \bar{S}_{ij}$  is the shear production;  $B = -\frac{g v_\theta}{\Theta} \frac{\partial \bar{\Theta}}{\partial z}$  is the buoyant production;  $\varepsilon = C_\varepsilon k_{\text{SGS}}^{3/2} / l$  is the dissipation rate; and  $\delta_{ij}$  is the Kronecker delta function.

The further parameterization for new terms is required to close the turbulence model. The length scale  $l$  is estimated as a function of the local grid size but damped near the walls using the van Driest damping functions to prevent excessive dissipation of TKE near the walls [42]. The length scale, far from the walls, where the damping functions are used, is formulated as

$$l = C_\Delta (\Delta x \Delta y \Delta z)^{1/3}, \quad (2.5)$$

where  $C_\Delta$  is a parameter to control  $l$  and therefore the SGS model. The turbulence model is closed using parameterizations for the remaining quantities including the turbulent viscosity,  $\nu_T = C_k k_{\text{SGS}}^{1/2} l$ , and the turbulent thermal viscosity,  $v_\theta = \nu_T / \text{Pr}_T$ .  $C_k$  is taken to be 0.094,  $C_\varepsilon$  is taken to be 1.048, and  $\text{Pr}_T$ , the turbulent Prandtl number, is taken to be 0.85.

## 2.2. Synthetic Vortex Method

A synthetic vortex method is used in the present VLES model to generate turbulence in the inlet section of the numerical domain. The vortex method used here was originally developed by Sergent [13] and has been continually improved until recently [14–16]. The main concept behind the vortex method is to generate velocity fluctuations in the form of synthetic vortices or eddies derived from the mean statistical information about the flow as a function of space (height above ground) and time. The controlling parameters are the number of vortices, the size of each vortex, the vorticity (or the equivalent velocity field characterizing each vortex), and the lifetime of vortices [15]. The vortices are two-dimensional with their vorticity vector being parallel to the streamwise direction. A schematic representation of the vortex generation is shown in Fig. 1a. The theory is fully developed in the literature [13–16] and provides the velocity fluctuation field for a given time step described by

$$\mathbf{u}(\mathbf{x}) = \frac{1}{2\pi} \sum_{i=1}^N \Gamma_i \frac{(\mathbf{x}_i - \mathbf{x}) \times \mathbf{s}}{|\mathbf{x}_i - \mathbf{x}|^2} \left( 1 - e^{-\frac{|\mathbf{x}_i - \mathbf{x}|^2}{2(\sigma_i(\mathbf{x}_i))^2}} \right) e^{-\frac{|\mathbf{x}_i - \mathbf{x}|^2}{2(\sigma_i(\mathbf{x}_i))^2}}, \quad (2.6)$$

where  $\mathbf{u}$  is velocity perturbation at the model inlet that is later superimposed on the mean inlet velocity,  $\mathbf{x}$  is position vector on the inlet boundary,  $N$  is the number of vortices to be inserted at the inlet (in the present work  $N = 200$  exclusively),  $i$  is the index for the current vortex,  $\Gamma_i$  is the circulation for the current vortex,  $\mathbf{x}_i$  is the position vector for the center of the current vortex,  $\mathbf{s}$  is the unit vector along the streamwise direction, and  $\sigma_i(\mathbf{x}_i)$  is the radius of the current vortex. Assuming that the flow is in the  $+x$  direction and

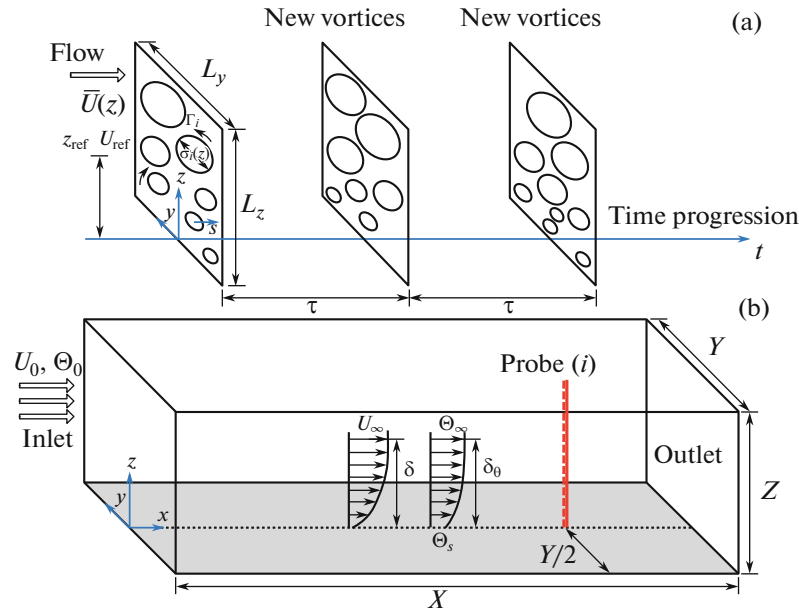


Fig. 1. Schematics of (a) vortex generation in the synthetic method and (b) computational domain.

the wall-normal direction is  $+z$ , a power-law profile is used to fit the mean velocity profile at the inlet [43] given by

$$\bar{U}(z) = U_{\text{ref}} \left( \frac{z}{z_{\text{ref}}} \right)^\alpha, \tag{2.7}$$

where  $z_{\text{ref}}$  is the reference height,  $U_{\text{ref}}$  is the reference velocity, and  $\alpha = 1/\ln(z_{\text{ref}}/z_0)$  is an exponent parameterized as a function of  $z_{\text{ref}}$  and aerodynamic roughness length  $z_0$  [5].

The size of energy-containing vortices is parameterized using a mixing length approach such that [9]

$$\frac{1}{\sigma(z)} = \frac{1}{\sigma_{\text{max}}} + \frac{1}{\kappa(z + z_0)}, \tag{2.8}$$

where  $\kappa = 0.41$  is the von Kármán constant and  $\sigma_{\text{max}}$  is the size of the greatest energy-containing vortex based on the characteristic length for the inlet boundary  $L$  [9]. We relate  $\sigma_{\text{max}}$  and  $L$  using a constant  $a_\sigma$ , to be adjusted later, with  $\sigma_{\text{max}} = a_\sigma L$ .

Using the scaling analysis, a characteristic time for the energy-containing vortices can be estimated. For the largest energy-containing eddies having the characteristic velocity  $U_0$  and the length scale  $\ell_0 = \sigma_{\text{max}}$  the characteristic time scale can be derived as

$$\tau_0(\ell_0) = \left( \frac{\ell_0^2}{\varepsilon} \right)^{1/3}, \tag{2.9}$$

where  $\varepsilon$  is the dissipation rate fully described and parameterized in [9]. This time scale is not representative for all energy-containing vortices, but only the largest ones. It is possible to define a representative time scale for all energy-containing eddies assuming a constant  $a_\tau$ , to be adjusted later, with  $\tau = a_\tau \tau_0(\ell_0)$ .

For the inlet temperature, the following power-law profile is used

$$\bar{\Theta}(z) = (\Theta_\infty - \Theta_s) \left( \frac{z}{z_{\text{max}}} \right)^\alpha + \Theta_s, \tag{2.10}$$

where  $\Theta_\infty$  is the far-field temperature on the boundary layer top,  $\Theta_s$  is the surface temperature,  $z_{\text{max}}$  is the height of the top of the domain, and  $\alpha$  is an exponent parameterized as a function of aerodynamic rough-

ness length, as described earlier in Eq. (2.7). The parameterization for the turbulence intensity profile and the vortex circulation at the inlet is not described here due to the space limitation and can be found in [9].

### 2.3. Wall Function Formulation

In order to economize the CFD simulations near the wall, velocity and temperature wall functions are used in the current VLES model. For velocity, an environmental flow wall function proposed by Raupach et al. [29] is described in the form:

$$U^+ = \frac{1}{\kappa} \ln \left( \frac{z + z_0}{z_0} \right) \approx \frac{1}{\kappa} \ln \left( \frac{z}{z_0} \right), \quad (2.11)$$

where  $\kappa = 0.41$  is the von Kármán constant. This wall function is known as `nutkAtmRoughWallFunction` in OpenFOAM.

The wall function for the temperature used in the current VLES model is inspired from [5]; it correlates the quantity  $\Theta^+ = (\Theta_s - \Theta) \rho c_p u_\tau / q_s$  (where  $q_s$  is the surface heat flux) and the logarithm of  $z^+$  via a linear relationship as follows:

$$\Theta^+ = \frac{1}{\kappa_\theta} \ln(z^+) + B_\theta, \quad (2.12)$$

where  $\kappa_\theta = 0.48$  is the thermal von Kármán constant and  $B_\theta = 3.9$  is a turbulence model constant. However, it is more common to formulate  $\Theta^+$  as a function of  $U^+$ , as follows:

$$\Theta^+ = \text{Pr}_T(U^+ + \text{Pr}_f), \quad (2.13)$$

where  $\text{Pr}_T = 0.85$  is the turbulent Prandtl number and  $\text{Pr}_f$  is described in [30]. This wall function is known as `alphatJayatillekeWallFunction` in OpenFOAM.

For TKE, the following wall function which is known as `kqRWallFunction` in OpenFOAM was used [41]

$$k_{\text{SGS}} = \frac{u_\tau^2}{C_\mu^{1/2}}, \quad (2.14)$$

where  $C_\mu = 0.09$  is a constant.

## 3. NUMERICAL DETAILS

### 3.1. Computational Domain and Grid Generation

A schematic of the computational domain is shown in Fig. 1b. The computational domain length, width, and height are  $X = 5$  m,  $Y = 1.5$  m, and  $Z = 1.2$  m, respectively. This domain has the same cross section as the wind tunnel used in Ohya [44]. The airflow is in the  $+x$  direction with the reference velocity and temperature set at the inlet, as shown in Fig. 1b. The typical velocity and temperature boundary layer profiles are drawn in this figure for illustration purposes. Six vertical solution profiles, each with multiple individual probes, are envisioned in the numerical domain for monitoring the simulation results. A sample profile can be seen in Fig. 1b. All six profiles are located at the mid-width of the domain,  $y = 0$ , covering the entire vertical height from  $z = 0$  to 1.2 m, and are spaced along the streamwise direction from  $x = 0$  to 5 m with 1-m increments.

Four numerical grids having different resolutions are used in this study to investigate the results of the VLES model as a function of the grid size. These grids, whose details are given in Table 1, range from very fine resolution with 1000000 control volumes to very coarse resolution with 62500 control volumes. The result of the grid resolution study will be presented in Table 1. The grid spacings in the  $x$  and  $y$  directions are uniform, while in the  $z$  direction, spacing is varied and it is clustered near the wall. The grid is generated using the `blockMesh` utility provided in OpenFOAM. The wall-adjacent grid height is tightly controlled and separately varied, independent of grading in the interior of the domain, so that the effect of using SGS model and wall functions can be studied independently. Values for  $z^+$  in the first layer are reported in Subsection 4.2, where the wall functions are used; otherwise, for wall-resolving simulations (Subsection 4.1)  $z^+ < 1.5$ .

**Table 1.** Numerical grids used for the current VLES simulations

Grid level	Description	$N_x - N_y - N_z$	$N_{\text{total}}$
I	Very fine	100 – 100 – 100	1000000
II	Fine	100 – 75 – 75	562500
III	Coarse	100 – 50 – 50	250000
IV	Very coarse	100 – 25 – 25	62500

### 3.2. Boundary Conditions

In the inlet section of the numerical domain, two separate power-law profiles for velocity and temperature, described by Eqs. (2.7) and (2.10), respectively, are used to generate the inlet profiles. For turbulence fluctuations, however, the synthetic vortex method is used to generate the turbulent fluctuations for velocity only, independent of the temperature, at the inlet as described by Eq. (2.6). As shown below, the solution adapts to turbulence at downstream for both velocity and temperature fluctuations. In the outlet section and at the top boundary the zero-gradient condition is used for all flow variables. The cyclic condition is used on the front and back sides of the numerical domain for all solution variables. At the bottom of the numerical domain, the no-slip condition is used for the velocity, and the constant temperature is used for the temperature.

For SGS TKE, the `atmBoundaryLayerInletK` boundary condition is used at the inlet. This condition assumes that the entire inlet boundary is in the inertial surface layer of ABL such that the friction velocity and TKE are independent of height [3]. This boundary condition first calculates the friction velocity, assuming the log-law, as

$$u_\tau = \frac{\kappa U_{\text{ref}}}{\ln\left(\frac{z_{\text{ref}} + z_0}{z_0}\right)}, \quad (3.1)$$

and then computes a uniform SGS TKE as  $k_{\text{SGS}} = u_\tau^2 / C_\mu^{1/2}$ , where  $C_\mu = 0.09$  is a constant. At the outlet, the zero-gradient condition is used for SGS TKE. At the wall, two conditions are possible, either zero value for wall-resolving simulations or the `kqRWallFunction` boundary condition when using the standard wall functions for rough surfaces. These two different wall conditions are used in this work to study the effect of wall functions on VLES results, to be discussed in Subsection 4.2.

For the turbulent viscosity, the zero-gradient condition is used in both inlet and outlet sections. At the wall, two conditions are possible, either zero-gradient for wall-resolving simulations or the `nutkAtmRoughWallFunction` boundary condition for rough surfaces. This condition modifies the turbulent viscosity near the surface such that

$$\nu_T = \nu \left( \frac{z^+ \kappa}{\ln \bar{E}} - 1 \right), \quad (3.2)$$

where  $\bar{E} = (z + z_0)/z_0$ . The temperature wall function described by Eq. (2.13) modifies the turbulent thermal diffusivity near the wall in the following form:

$$\alpha_\theta = \alpha \left( \frac{z^+ \kappa}{\left(\frac{\text{Pr}_T}{\text{Pr}}\right) \ln \bar{E} + \kappa} - 1 \right), \quad (3.3)$$

where  $\alpha$  is molecular thermal diffusivity. This boundary condition is known as `alphatJayatillekeWallFunction` in OpenFOAM.

### 3.3. Numerical Schemes

A second-order implicit backward time scheme is used, and all gradient schemes are based on the second-order Gaussian integration with linear interpolation. All Laplacian schemes are based on the corrected Gaussian integration with linear interpolation, which provides an unbounded, second-order, and

conservative numerical behavior. Divergence schemes are based on Gaussian integration with linear or upwind interpolation, depending on the variable of interest [41].

Throughout all simulations, time steps are chosen so that the maximum Courant number satisfies the condition  $Co = \Delta t |\bar{U}| / \Delta x < 1$ . The pressure matrix is preconditioned by the diagonal incomplete Cholesky technique and solved by the preconditioned conjugate gradient solver. Other variables are preconditioned by the diagonal incomplete-lower-upper technique and solved by the preconditioned bi-conjugate gradient solver. The pressure-linked equations are solved by a hybrid method consisting of two algorithms of the pressure-implicit split-operator method and the semi-implicit method [41].

There is a large amount of research on the effect of numerical schemes on scale resolving simulations [45–50]. Vreman et al. [45] examined the effect of a few numerical schemes including second- and fourth-order central differences and a spectral method on the LES of the temporal mixing layer. They concluded that the spectral scheme gives somewhat better results than the finite-difference schemes, while it requires higher computational effort and time. Moin [46] discussed the details of two widely-used numerical schemes for LES of complex configurations, namely, the immersed boundary method and an unstructured mesh scheme. The interaction between numerical discretization and SGS modeling was studied in [48]. Adams et al. [48] used implicit SGS models based on finite-volume discretizations that allows for a full merge of discretization and the SGS model. They proposed a nonlinear discretization scheme for the SGS model in regions, where the flow is turbulent, and a second-order accurate discretization scheme in regions, where the flow is laminar. The effect of convergence criteria and time step size on LES of a specific wall bounded flow was investigated in [49]. It was found that the simulations with the weaker convergence criteria are more computationally efficient. Fauconnier et al. [50] studied the numerical errors and the modeling errors of explicit and implicit dynamic finite difference schemes in LES of the three-dimensional Taylor–Green vortex flow. They reported that dynamic finite-difference schemes achieved an optimal accuracy for all resolved scales of motion in the flow at any time and resulted in lower numerical errors than the standard asymptotic finite difference schemes. The numerical schemes used in the current study resulted in reasonably well predictions of various flow conditions. Therefore, the effect of different numerical schemes on the current simulations has not been examined and the reader is encouraged to study other relevant resources found in [45–50].

#### 4. RESULTS AND DISCUSSION

The results of the VLES model for the stratified stable ABL are presented in this section. Four different stability cases detailed in Table 2 were simulated and compared against the experimental measurements of Ohya [44]. The first two cases represent weakly stable regimes and the last two cases have characteristics of strongly stable flows [44]. This experimental study was used as the evaluation dataset for the model performance in this paper. The experiments were conducted in a thermally stratified wind tunnel having a chain roughness with an average height of  $h = 5$  mm, equivalent to an aerodynamic roughness length of approximately  $z_0 = 0.55$  mm [44]. Throughout this paper, several variables predicted by the VLES model on the vertical profile located at  $x = 4$  m (see Subsection 3.1 and Fig. 1b) are compared with the experimental measurements of Ohya [44]. The stability parameter used in Table 2 and in [44] is the bulk Richardson number based on the boundary-layer height

$$Ri_\delta = \frac{g}{\Theta_0} \frac{\delta(\Delta\Theta)}{U_0^2}, \quad (4.1)$$

where  $\Delta\Theta = \Theta_\infty - \Theta_s$  is the temperature difference between the wall and the boundary-layer top and  $\Theta_0 = (\Theta_\infty + \Theta_s)/2$  is the average temperature.

The results of the VLES model in this section are presented in a systematic order to demonstrate how the numerical parameters of the model were adjusted with respect to the model accuracy. The performance of the VLES model for wall-resolving simulations in four different stability cases is assessed in Subsection 4.1. This allows us to test the model for its synthetic and SGS parameterizations, independent of wall functions, in a succession of coarse grids. Examining the model performance with wall functions is conducted as the next step of the current systematic numerical investigations presented in Subsection 4.2.

##### 4.1. Wall-Resolving Simulations for SBL

This section contains the wall-resolving simulations for four different stability cases described in Table 2. First, a series of sensitivity studies on the numerical model was conducted for the stability case 1; it is

**Table 2.** Thermal stability cases simulated in this study

Case	1	2	3	4
$U_\infty$ [m s <sup>-1</sup> ]	1.83	1.29	1.01	0.91
$\Delta\Theta$ [K]	27.4	27.4	28.7	43.3
$Re_\delta$	121127	85736	67450	54375
$Ri_\delta$	0.12	0.24	0.40	0.74
$\delta$ [m]	1.08	1.035	1.01	0.885
Number of inlet vortices per $\delta^2$	129	119	113	87
Number of grid cells per $\delta^3$	34992	31422	29922	21930

described in Subsection 4.1.4 to 4.1.3. Following the reductionist approach of the present work, the results of these sensitivity studies make it possible to apply the VLES model with a limited number of input variables for the stability analysis of the flow carried out in Subsection 4.1.4 and 4.1.5.

#### 4.1.1. Numerical Grid Study

It is expected that the VLES model should be able to simulate the mean properties of the flow, turbulence variances, and turbulence fluxes (covariances) accurately for coarse grids. Therefore, one of the crucial sensitivity studies for the VLES model is to examine the performance of the model over a series of numerical grids from very fine to very coarse grid resolutions. The performance of the VLES model for four different numerical grids detailed in Table 1 is presented in Figs. 2a to 2c. Due to the space limitations, only selected variables are presented in this figure. Since it is too computationally expensive to conduct the grid sensitivity study for all stability cases, it was only performed for one stability case. The experimental measurements of [44] are also plotted in this figure for comparison. It is evident from Figs. 2a–2c that the results of the numerical model agree reasonably well with the experimental observations for a grid level as coarse as grid level III. The very coarse grid level IV shows large deviations from the experimental data, especially for turbulence variables. These results suggest that the grid level III is the coarsening limit for preserving the boundary-layer mean and turbulence features. Therefore, this grid is used in the rest of the numerical simulations of the present study.

In addition to this grid study, it was ensured that the grid size is adequate to resolve the turbulence structures. This was achieved by comparing the grid size with the that of the greatest energy-containing eddy, the turbulence integral length scale. The integral length scale of the turbulent eddies was estimated to be in the range from 0.15 to 0.7 m for the four stability cases in the interior of the domain ( $z > 0.05\delta$ ), increasing as moving away from the wall. The procedure for estimating the integral length and time scales was adopted from [5, 51]. The numerical grid used in the current simulations has constant  $\Delta x = 0.05$  m and  $\Delta y = 0.03$  m, while the grid size in the  $z$  direction is variable, as it is clustered near the wall. The grid spacing in the  $z$  direction,  $\Delta z$ , is 0.001 m adjacent to the wall to 0.095 m in the free-stream area. From this information, it could be concluded that the grid size was adequate for the turbulent flow simulations. Regarding the flow time scales, the time step of 0.005 s and an averaging time of 100 s were used to average different variables in this study. The integral time scale was estimated to be in the range of 0.14 to 0.76 s for the four stability cases in the interior of the domain ( $z > 0.05\delta$ ). Considering the time step being about 28 to 152 times smaller than the integral time scales and the averaging time being at least 100 times longer than the integral time scales, it can be stated that the time step and averaging time used in our simulations were adequate to resolve the turbulence structures.

#### 4.1.2. Model Refinement for Synthetic Vortex Method

As discussed earlier, the synthetic vortex method used to generate the inlet turbulence has a reductionist approach that allows the method to control the turbulence characteristics in the numerical domain using only two parameters,  $a_\sigma$  and  $a_\tau$ . The sensitivity of the model to these two parameters is studied in this section. First, the influence of  $a_\sigma$ , the numerical parameter controlling the size of eddies generated at the inlet, on the results of the VLES model is examined. Then, the model performance with respect to  $a_\tau$ , the numerical parameter regulating how frequently new eddies are sampled at the inlet, is studied.

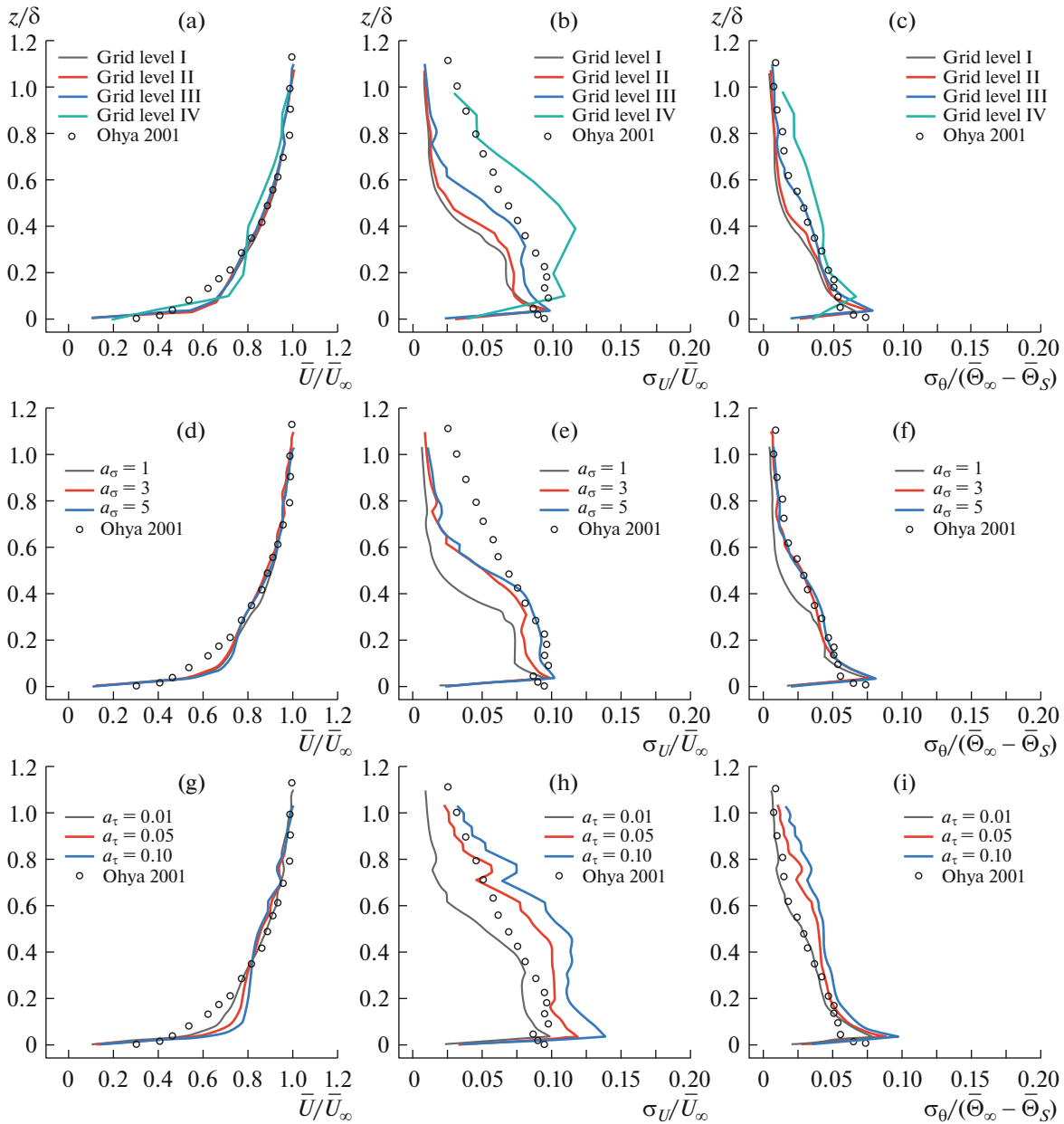


**Fig. 2.** Sensitivity of the VLES model to grid size (a–c),  $a_\sigma$  (d–f), and  $a_\tau$  (g–i) for mean horizontal velocity (a, d, g), horizontal velocity fluctuations (b, e, h), and temperature fluctuations (c, f, i).

Figures 2d to 2f show that the mean velocity is not affected by varying  $a_\sigma$ . On the other hand, increasing the value of  $a_\sigma$  from 1 to 5 increases the turbulence statistics noticeably. This can be explained by the fact that the higher  $a_\sigma$  values correspond to the larger eddies that are more energetic and add to the turbulence levels in the simulated flow. Although it is difficult to find the perfect value of  $a_\sigma$  that would match the experimental data closely within the entire height of the boundary layer, it seems that  $a_\sigma = 3$  provides the best agreement with the experiment.

The sensitivity analysis of the synthetic vortex method to  $a_\tau$  presented in Figs. 2g to 2i shows the same trends, as those observed for  $a_\sigma$ , i.e., the negligible sensitivity for the mean variables and a high sensitivity for the turbulence statistics. Considering the fact that  $a_\tau$  controls the lifetime of the largest energy-containing eddies at the inlet, it is expected that high values of  $a_\tau$  should result in greater magnitudes of the

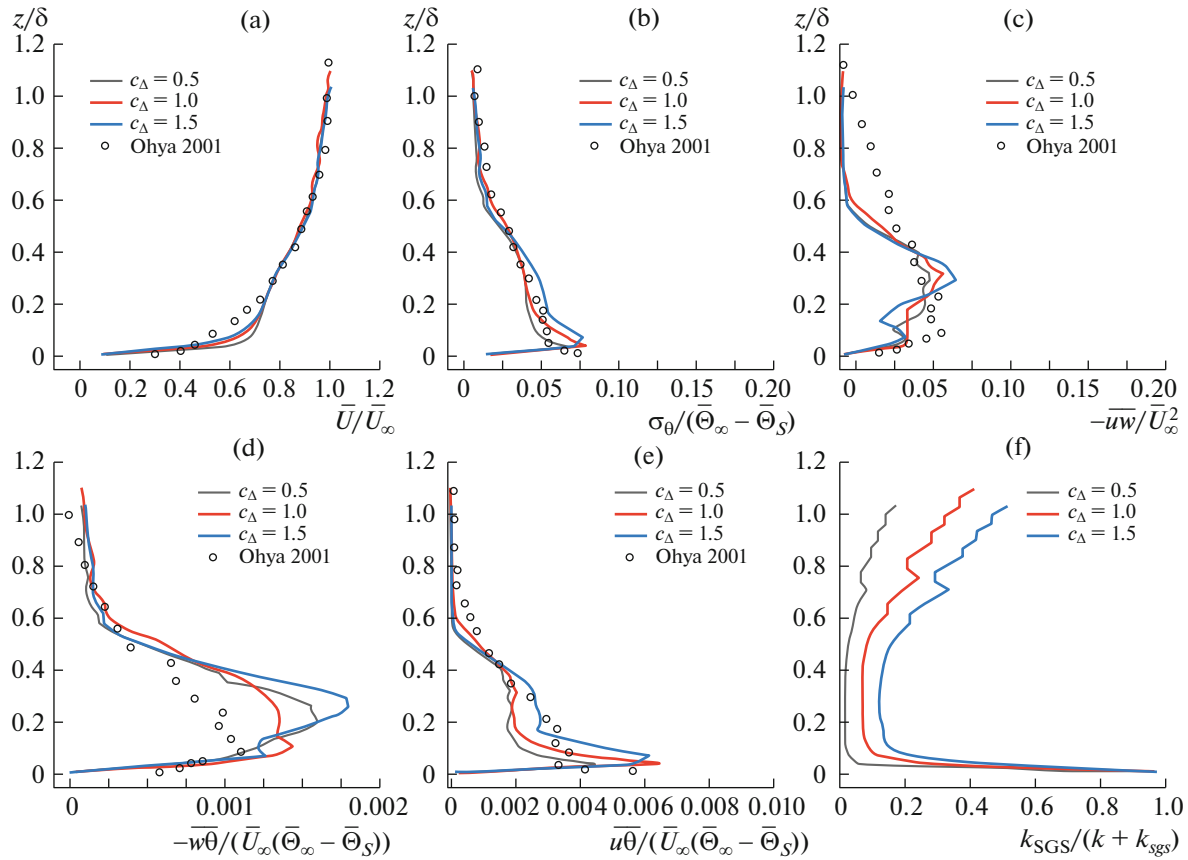


**Fig. 3.** Sensitivity of the VLES model to  $C_\Delta$  for (a) mean horizontal velocity, (b) temperature fluctuations, (c) Reynolds shear stress, (d) vertical turbulent heat flux, (e) horizontal turbulent heat flux, and (f) the ratio of modeled TKE to total TKE.

turbulence statistics. In an overall look, from Figs. 2g to 2i it can be observed that the wall-resolving VLES model has the best agreement with the wind-tunnel observations, when  $a_\tau = 0.01$ .

#### 4.1.3. Model Refinement for SGS Model

The sensitivity of the SGS model is tested by varying the constant  $C_\Delta$  that controls the SGS length scale  $l$  (see Eq. (2.5)), as shown in Fig. 3. This figure shows that different values of  $C_\Delta$  have marginal effects on the mean variables (Fig. 3a) and turbulence variances (Fig. 3b). However, the influence of the  $C_\Delta$  variation on turbulent fluxes of momentum (Fig. 3c) and heat (Figs. 3d and 3e) is greater. This can be explained by the fact that this parameter controls the transport phenomena at subgrid scales by controlling the subgrid mixing length. It can be observed from Figs. 3d and 3e that all the three values of  $C_\Delta$  overestimate the vertical turbulent heat flux in the bottom half of the boundary layer, while they all predict the horizontal turbulent heat flux with reasonable accuracy. This makes the selection of the perfect value for this parameter somewhat difficult. Therefore, an analysis of the ratio of the modeled TKE to the total TKE can be helpful in this selection process. This ratio plotted in Fig. 3f shows that with increasing  $C_\Delta$  the modeled to the total TKE ratio increases in the interior of the boundary layer domain. This ratio is large near the wall, which might be expected, since the flow is closer to the viscous sublayer. It was found that for a successful VLES, at most 20% of the TKE in the interior of the domain should be modeled and more than 80% should be resolved [40]. Considering this criterion in Fig. 3f, along with the information gathered in Figs. 3a to 3e, it seems that  $C_\Delta = 1$  is the most suitable value for this numerical model in wall-resolving simulations.

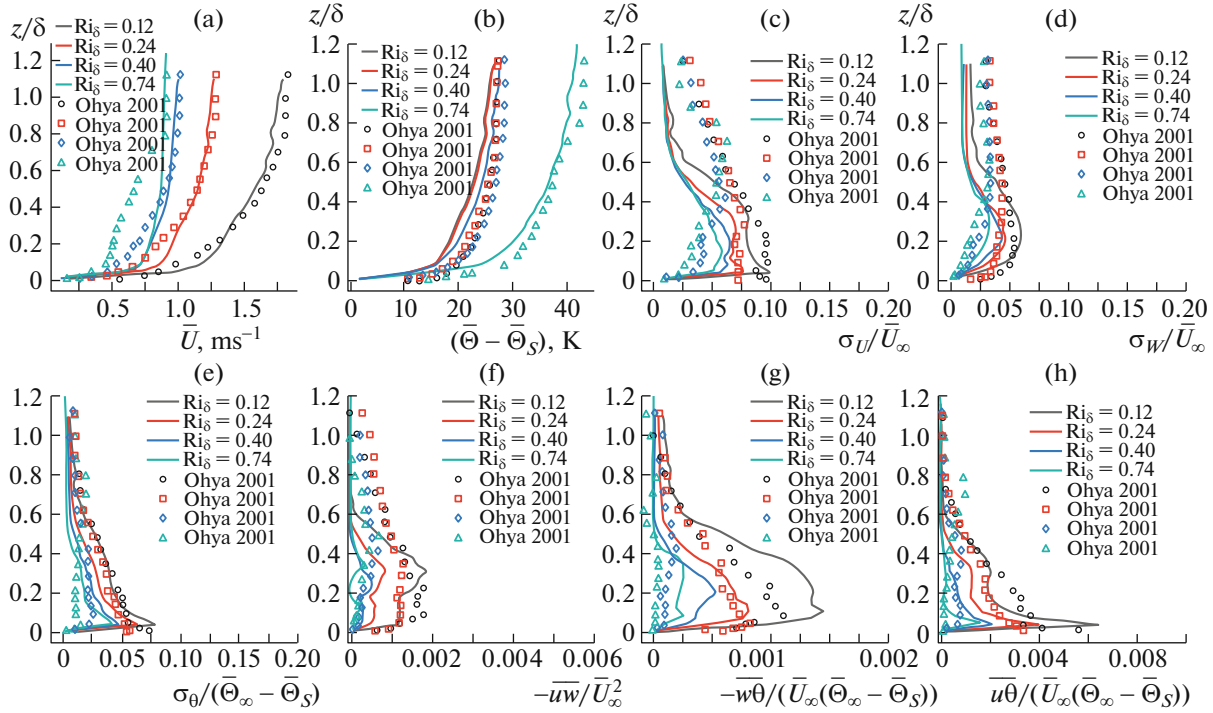


**Fig. 4.** Wall-resolving simulations for four stability cases, (a) mean horizontal velocity, (b) mean temperature, (c) horizontal velocity fluctuations, (d) vertical velocity fluctuations, (e) temperature fluctuations, (f) Reynolds shear stress, (g) vertical turbulent heat flux, and (h) horizontal turbulent heat flux.

#### 4.1.4. Thermal Stability Cases

After adjusting the values for different numerical parameters studied in the previous sections, the VLES code was run to examine the effect of thermal stratification on the ABL. Figure 4 shows the results of wall-resolving simulations for the four different stability cases described in Table 2, as well as the comparison of the results with the experimental work [44]. These simulations were run on grid level III with the synthetic vortex method numerical parameters  $a_\sigma = 3$  and  $a_\tau = 0.01$  and the SGS numerical parameter  $C_\Delta = 1$ .

As for the mean velocity profiles, it can be seen from Fig. 4a that with increase in the stability level from a weakly stable case ( $Ri_\delta = 0.12$ ) to a strongly stable case ( $Ri_\delta = 0.74$ ) the velocity deficit increases under the effect of thermal stratifications. The mean temperature profiles plotted in Fig. 4b are shifted toward greater values with increase in the stability while, this increase being small for the first three stability cases but fairly large for the strongly stable case of  $Ri_\delta = 0.74$ .

As for turbulence fluctuations of the horizontal velocity, the vertical velocity, and the temperature shown in Figs. 4c to 4e, it is evident that increasing the thermal stability reduces the turbulent fluctuations. This is due to the fact that the buoyancy forces caused by the thermal stratification have a stabilizing effect on the boundary layer by suppressing the turbulence. The buoyancy forces, especially, reduce fluctuations in the vertical component of velocity, as reported in [1]. This can be seen in the present work as well, in Figs. 4c and 4d, where the turbulent fluctuations of  $w$  are almost half of the turbulent fluctuations of  $u$  component for these SBL flows.

As for turbulent momentum and heat fluxes, the stabilizing effect of the thermal stratification with increase in the Richardson number can be clearly observed in Figs. 4f to 4h. Another trend evident in both groups of turbulent fluctuations in Figs. 4c to 4e and turbulent fluxes in Figs. 4f to 4h is the different behavior of the weakly stable cases,  $Ri_\delta = 0.12$  and  $0.24$ , and strongly stable cases,  $Ri_\delta = 0.40$  and  $0.74$ . The two weakly stable cases have consistently nonzero values in the bottom half of the boundary layer before approaching zero at a small height above the wall, about  $z = 0.05\delta$ . For the two strongly stable cases, this decline toward zero values starts at greater heights with values very close to zero. This is an indication of turbulence suppression under strong thermal stratifications. This turbulence suppression can also be observed in Fig. 5, where instantaneous contours of the vorticity  $y$ -component are plotted for the

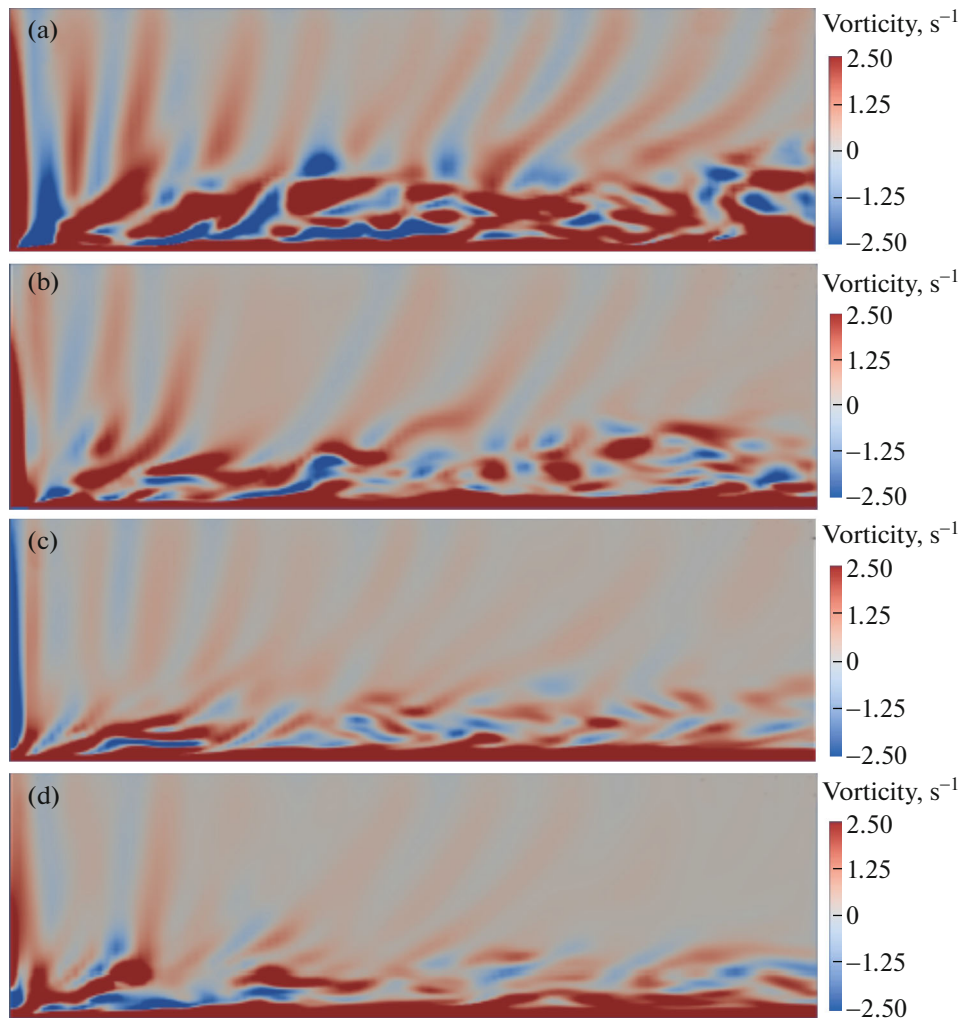


**Fig. 5.**  $y$ -component of vorticity contours in the central  $x - z$  plane for four stability levels of Richardson number ( $Ri_\delta$ ): (a) 0.12, (b) 0.24, (c) 0.40, and (d) 0.74.

four thermal stability cases at the central  $x - z$  plane. As evident in this figure, in the two weakly stable cases ( $Ri_\delta = 0.12$  and  $0.24$ ), a large portion of the flow domain is dominated by large eddies as can be inferred by the high vorticity levels. In contrast, for the two strongly stable cases ( $Ri_\delta = 0.40$  and  $0.74$ ), the high vorticity areas are limited to small regions near the wall, while the turbulent motions in interior of the domain are suppressed.

In an overall look at Fig. 4, it can be said that the agreement between the current numerical results and experimental observations [44] is fair for both mean and turbulence profiles. Although there are some discrepancies between the VLES model and the experimental data, the overall behavior of the SBL at different stability levels is predicted well using this model.

#### 4.1.5. Spectral Analysis for Wall-Resolving Simulations

Although CFD models are mainly evaluated based on their predictions of mean and turbulence variables, a successful spectral analysis of turbulent fluctuations provides a higher degree of confidence in a numerical model. The spectral analysis of the four stability cases simulated by the wall-resolving VLES model is presented in Figs. 6a to 6c for turbulent fluctuations of the horizontal velocity, the vertical velocity, and the temperature, respectively. The cospectral analysis of the Reynolds shear stress  $\overline{uw}$ , the vertical heat flux  $\overline{w\theta}$ , and the horizontal heat flux  $\overline{u\theta}$  is presented in Figs. 6d to 6f for the same stability cases. The

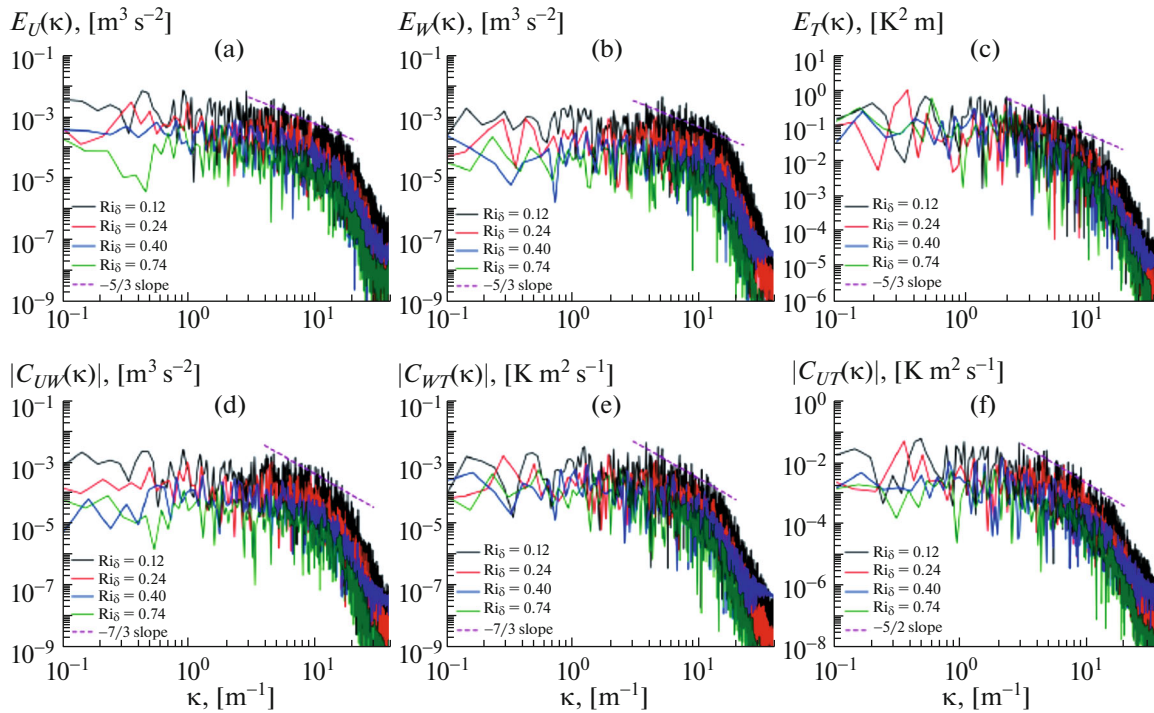


**Fig. 6.** Spectral analysis for wall-resolving simulations for four thermal stability cases at  $z = 0.25$  m for (a) horizontal velocity fluctuations, (b) vertical velocity fluctuations, (c) temperature fluctuations, (d) Reynolds shear stress, (e) vertical turbulent heat flux, and (f) horizontal turbulent heat flux.

details of spectral analysis approach carried out for the current simulation data can be found in [3]. For anisotropic ABL flows, it has been suggested that in the inertial subrange the slope of the spectral energy density  $E(\kappa)$  for velocity and temperature fluctuation components versus the wavenumber  $\kappa$  in the log-log scale is  $-5/3$  (Kolmogorov spectrum) [3, 52]. The slope of the cospectral energy density  $C(\kappa)$  for velocity fluctuations along streamwise ( $x$ ) and vertical ( $z$ ) directions versus the wavenumber  $\kappa$  in the log-log scale is approximately  $-7/3$  [52]. For the cospectral energy density of the turbulent vertical and horizontal heat fluxes, this slope in the inertial subrange is  $-7/3$  and  $-5/2$ , respectively [52]. These slopes for the corresponding variables are plotted in Fig. 6 for comparison purposes.

It can be observed from Figs. 6a to 6c that the spectral content of turbulent velocity and temperature fluctuations is resolved by the VLES model for almost two orders of magnitude of wave numbers. The inertial subrange is partially matched, while the smaller scales of the inertial subrange are modeled (not resolved) resulting in the sharp drop and truncation of the spectra. Moreover, the spectral data follow the sample slope line of  $-5/3$  reasonably well for the inertial subrange. Figures 6a to 6c also show that an increase in the thermal stability results in reduction of the energy spectral density amplitude, which can be attributed to turbulence suppression by buoyant forces.

The cospectra of turbulent momentum and heat fluxes are also resolved for almost two orders of magnitude of wave numbers and partially matched for the inertial subrange (see Figs. 6d to 6f). These graphs also show a good agreement between the cospectral data and the log-log slope for the inertial subrange. It is evident in Figs. 6d to 6f that the cospectral density between each two corresponding parameters is reduced by increasing the Richardson number for the four stability cases simulated.

#### 4.2. VLES with Wall Function

The simulation results of the VLES model over a rough surface using two wall functions for velocity and temperature to further economize the model are discussed in this section. Grid level III was chosen for these simulations and the adjusted values for synthetic vortex method and SGS model numerical parameters found for the wall-resolving simulation in the previous section were used here ( $a_\sigma = 3$  and  $C_\Delta = 1$ ) except for the parameter controlling the vortex time scale, where a greater value  $a_\tau = 0.05$  was

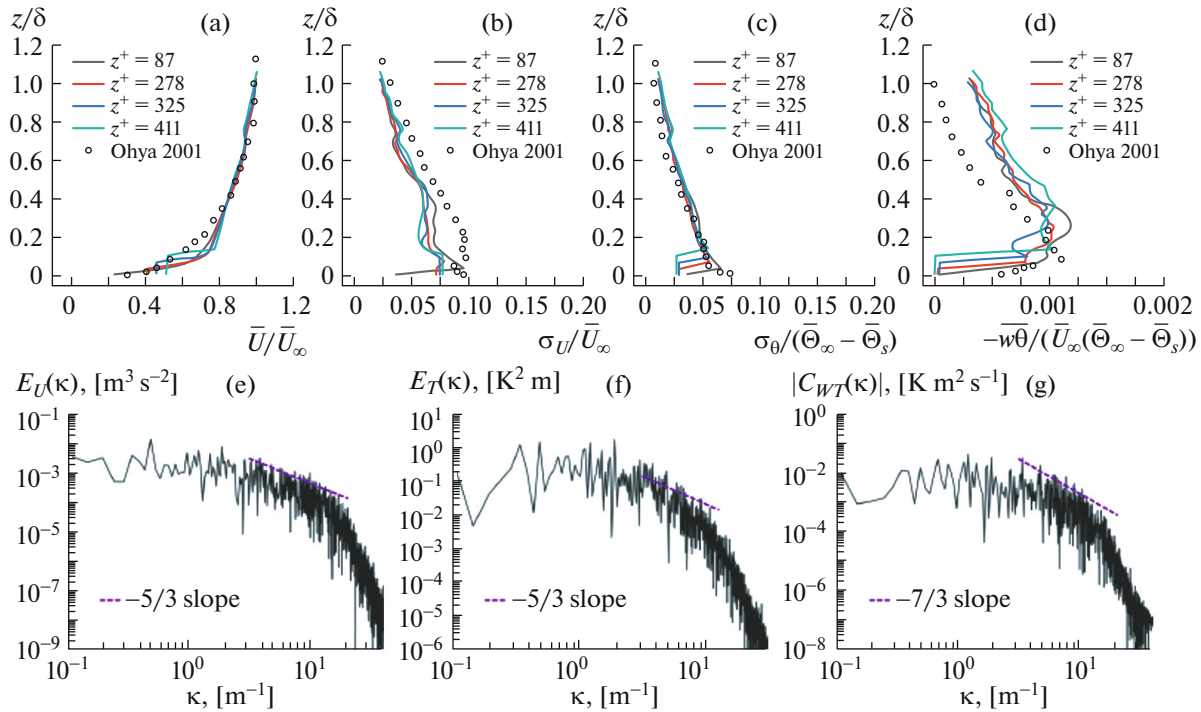


**Fig. 7.** VLES with wall functions for four different  $z^+ = 87, 278, 325,$  and  $411$  for stability case 1, (a) mean horizontal velocity, (b) horizontal velocity fluctuations, (c) temperature fluctuations, and (d) vertical turbulent heat flux and spectral analysis for stability case 1 at  $z = 0.25$  m for (e) horizontal velocity fluctuations, (f) temperature fluctuations, and (g) vertical turbulent heat flux.

used. This greater value of  $a_\tau$  was selected here since in the simulations with wall functions a higher time scale for large eddies needs to be assumed. This can be explained by the fact that when wall functions are used, turbulence generation near the walls is modeled rather than resolved, in which case eddy formation at some distance away from the wall occurs with a greater time constant. This implies that the TKE transfer from the wall to the outer layer starts with greater time constants and, therefore, it necessitates more model time iterations before new eddies are sampled at the inlet.

In CFD simulations with wall functions selecting the first layer grid height is of great importance. Therefore, the VLES model was run for four different values of the first layer grid height. Figures 7a to 7d show the sensitivity of the model to the variation of  $z_p$ , the mid height of the first computational cell for stability case 1. The  $z^+$  values corresponding to these four levels of the first layer grid heights are determined to be 87, 278, 325, and 411. The procedure for  $z^+$  calculation is explained in [9]. It can be seen in Figs. 7a to 7d that the current simulation results agree reasonably well with the experimental data [44] in the areas far from the wall for most of the mean and turbulence variables reported here, though some discrepancies are observable. For the near-wall regions, where the wall functions are modeling turbulence, it seems that the two lowest values of  $z^+$  (87 and 278) provide better agreements with the experimental data. Therefore, it can be suggested that  $z^+$  for the successful simulation of the ABL under thermal stratification should be smaller than 278. The decline in turbulence statistics near walls with the use of wall functions was already expected and, in fact, desired, because using the wall functions forces the simulations to model fluctuations rather than to resolve them. So this trend should not be interpreted as the weakness of the model. In fact, the synthetic method input parameters can be further adjusted to circumvent this, although this is beyond the scope of this study. Nevertheless, the errors of the model with the wall functions for the two lowest values of  $z^+$  are well within the range of the wall-resolving model errors.

The spectral analysis of the VLES with the wall functions in the numerical domain corresponding to  $z^+ = 278$  for stability case 1 is reported in Figs. 7e to 7g. Also plotted in this figure are the log–log slopes for the corresponding variables discussed in Subsection 4.1.5. For both velocity and temperature spectra and cospectra in Figs. 7e and 7g, it can be seen how the VLES model successfully resolves almost two orders of magnitude of wave numbers. The inertial subrange is partially matched for both spectral and

cospectral graphs. A fair agreement can also be observed for these spectra and cospectra with the corresponding slopes in the inertial subrange.

## SUMMARY

A VLES model was developed to simulate thermally-stratified atmospheric boundary layers. This model, utilizing a robust inlet turbulence generation technique, the synthetic vortex method, and coupled velocity/temperature wall functions, exhibits a reductionist approach to minimize the number of input parameters, which makes it a practical tool for industrial applications. A series of numerical investigations are performed to study the sensitivity of the model to several input parameters including the grid resolution, the parameters of the synthetic vortex method generating turbulence at the inlet, and the SGS model filter length. These sensitivity studies resulted in the model having realistic thermal-flow simulations of the mean and turbulence variables, while minimizing the computational cost. Moreover, the model was successful on a relatively coarse grid, a current limitation of many LES studies simulating thermally-stratified boundary layers.

A grid sensitivity study was performed to determine the coarsening limit of the numerical grid for the wall-resolving simulations by using four different grids ranging from very fine resolution with 1000000 control volumes to very coarse resolution with 62500 control volumes. It was found that a grid level having 250000 control volumes provided acceptable results, where more than 80% of the TKE was resolved in the interior of the numerical domain. The synthetic vortex method used to generate turbulence fluctuations at the inlet was refined by determining the optimal values for the numerical parameters controlling the length scale and time scale of the eddies generated at the inlet. The sensitivity of the SGS model was also studied by conducting a series of numerical runs for different values of the SGS model filter length. It was found that the group of numerical parameters of  $a_\sigma = 3$ , controlling the inlet eddy length scale,  $a_\tau = 0.01$  (0.05 with wall treatments), controlling inlet eddy time scale, and  $C_\Delta = 1$ , controlling the SGS filter length, on the grid with 250000 control volumes provided the best agreement with wind-tunnel measurements.

The performance of the model was evaluated against wind-tunnel observations for four different thermal stability levels ranging from weak (bulk Richardson number  $Ri_\delta = 0.12$ ) to strong ( $Ri_\delta = 0.74$ ) stability. The agreement between the current numerical model and the wind-tunnel data was fair for the mean velocity profile, the mean temperature profile, the variances, the turbulent momentum fluxes, and the turbulent heat fluxes. It was found that the buoyancy forces caused by thermal stratification stabilize the boundary layer by suppressing the turbulence fluctuations of velocity and temperature, as well as reducing the turbulence momentum and heat fluxes. Moreover, the model was further economized by implementing velocity and temperature wall functions. It was found that the VLES model is sensitive to the height of the first numerical grid layer adjacent to the wall, especially in simulating the near-wall region. While the output of the model was satisfactory for dimensionless wall units  $z^+ = 87$  and 278, some discrepancies with the experimental data were observed for the greater  $z^+$  values. For both wall-resolving simulations and simulations with wall functions, the spectral responses of the model for velocity components, temperature, momentum and heat fluxes were analyzed. It was found that the model is capable of successfully resolving the energy cascade for almost two orders of magnitude of wave numbers and partially matching the well-known log-log slopes in the inertial subrange.

The reductionist approach of the model, careful simulation set-up, systematic sensitivity studies, and fair evaluations against wind-tunnel experiments, make it suitable for industrial applications, where it is impractical to perform sophisticated high resolution simulations. Moreover, the current numerical parameters adjusted for the stable boundary-layer flows can help other researchers in their VLES development efforts. Future development of this model can extend to the simulation of transport phenomena in gas dispersion studies. Additionally, the model should be tested at full scale for atmospheric boundary-layer simulations. Developing the model for complex topographies with differential surface temperature is considered another long-term goal for this VLES model.

## ACKNOWLEDGEMENTS

The authors are indebted to Joel Best, Jeff Madge, and Matthew Kent from the IT group at the University of Guelph for setting up the simulation platforms. The authors acknowledge the assistance of Manoj Kizhakkaniyil in converting the OpenFOAM solver from version 3.0 to version 4.0. In-kind technical support for this work was provided by Rowan Williams Davies & Irwin Inc (RWDI). Useful discussions with Gonalo Pedro and Franoise Robe

at RWDI are acknowledged. Useful discussions with John D. Wilson and Thomas Flesch, Department of Earth and Atmospheric Sciences, University of Alberta, are acknowledged.

#### FUNDING

This work was supported by the Discovery Grant program (no. 401231) from the Natural Sciences and Engineering Research Council (NSERC) of Canada; Government of Ontario through the Ontario Centres of Excellence (OCE) under the Alberta-Ontario Innovation Program (AOIP) (no. 053450); and Emission Reduction Alberta (ERA) (no. 053498). OCE is a member of the Ontario Network of Entrepreneurs (ONE).

#### DECLARATION OF CONFLICTING INTERESTS

The Authors declare no potential conflicts of interest with respect to the research, authorship, and/or publication of this article.

#### REFERENCES

1. T. Van Buren, O. Williams, and A. J. Smits, "Turbulent boundary layer response to the introduction of stable stratification," *J. Fluid Mech.* **811**, 569–581 (2017).
2. J. Huang and E. Bou-Zeid, "Turbulence and vertical fluxes in the stable atmospheric boundary layer. Part I: A large-eddy simulation study," *J. Atmos. Sci.* **70**, 1513–1527 (2013).
3. R. B. Stull, *An Introduction to Boundary Layer Meteorology* (Kluwer, Dordrecht, 1988).
4. A. A. Aliabadi, M. Moradi, D. Clement, W. D. Lubitz, and B. Gharabaghi, "Flow and temperature dynamics in an urban canyon under a comprehensive set of wind directions, wind speeds, and thermal stability conditions," *Environ. Fluid Mech.* **19**, 81–109 (2019).
5. A. A. Aliabadi, *Theory and Applications of Turbulence: A Fundamental Approach for Scientists and Engineers* (Amir A. Aliabadi Publ., Guelph, 2018).
6. V. Kumar, J. Kleissl, C. Meneveau, and M. B. Parlange, "Large-eddy simulation of a diurnal cycle of the atmospheric boundary layer: Atmospheric stability and scaling issues." *Water Resource Res.* **42**(W06D09), 1–18 (2006).
7. J. Sandham and M. L. Waite, "Spectral energy balance in dry convective boundary layers," *J. Turbul.* **16**(7), 650–675 (2015).
8. B.-S. Han, J.-J. Baik, S.-B. Park, and K.-H. Kwak, "Large-eddy simulations of reactive pollutant dispersion in the convective boundary layer over flat and urban-like surfaces," *Boundary-Layer Meteorol.* **172**(2), 271–289, (2019).
9. A. A. Aliabadi, N. Veriotes, and G. Pedro, "A very large-eddy simulation (VLES) model for the investigation of the neutral atmospheric boundary layer," *J. Wind Eng. Ind. Aerodyn.* **183**, 152–171 (2018).
10. G. R. Tabor and M. H. Baba-Ahmadi, "Inlet conditions for large eddy simulation: A review," *Comput. Fluids* **39**(4), 553–567 (2010).
11. T. S. Lund, X. Wu, and K. D. Squires, "Generation of turbulent inflow data for spatially-developing boundary layer simulations," *J. Comput. Phys.* **140**(2), 233–258 (1998).
12. P. R. Spalart, "Direct simulation of a turbulent boundary layer up to  $Re_\theta = 1410$ ," *J. Fluid Mech.* **187**, 61–98 (1988).
13. M. E. Sergent, *Towards a coupling methodology between large eddy simulation and statistical models* (Ph.D. Thesis, École Centrale De Lyon, Lyon, France, 2002).
14. S. Benhamadouche, N. Jarrin, Y. Addad, and D. Laurence, "Synthetic turbulent inflow conditions based on a vortex method for large-eddy simulation," *Progr. Comput. Fluid Dyn.* **6**(1–3), 50–57 (2006).
15. F. Mathey, D. Cokljat, J. P. Bertoglio, and E. Sergent, "Assessment of the vortex method for large eddy simulation inlet conditions," *Progr. Comput. Fluid Dyn.* **6**(1–3), 58–67 (2006).
16. B. Xie, F. Gao, J. Boudet, L. Shao, and L. Lu, "Improved vortex method for large-eddy simulation inflow generation," *Computers Fluids* **168**, 87–100 (2018).
17. H. Aboshosha, A. Elshaer, G. T. Bitsuamlak, and A. El Damatty, "J. Wind Eng. Ind. Aerodyn." **142**, 198–216 (2015).
18. R. J. Beare and M. K. Macvean, "Consistent inflow turbulence generator for LES evaluation of wind-induced responses for tall buildings," *Boundary-Layer Meteorol.* **112**, 257 (2004).
19. S. R. de Roode, H. J. J. Jonker, B. J. H. Van De Wiel, V. Vertregt, and V. Perrin, "A diagnosis of excessive mixing in Smagorinsky subfilter-scale turbulent kinetic energy models," *J. Atmos. Sci.* **74**, 1495–1511 (2017).

20. J. Smagorinsky, "General circulation experiments with the primitive equations: I. The basic equations," *Mon. Weather Rev.* **91**, 99–164 (1963).
21. J. Fröhlich, C. P. Mellen, W. Rodi, L. Temmerman, and M. A. Leschziner, "Highly resolved large-eddy simulation of separated flow in a channel with streamwise periodic constrictions," *J. Fluid Mech.* **526**, 19–66 (2005).
22. X.-X. Li, R. E. Britter, T. Y. Koh, L. K. Norford, C.-H. Liu, D. Entekhabi, and D. Y. C. Leung, "Large-eddy simulation of flow and pollutant transport in urban street canyons with ground heating," *Boundary-Layer Meteorol.* **137**(2), 187–204 (2010).
23. A. A. Aliabadi, E. S. Krayenhoff, N. Nazarian, L. W. Chew, P. R. Armstrong, A. Afshari, and L. K. Norford, "Effects of roof-edge roughness on air temperature and pollutant concentration in urban canyons," *Boundary-Layer Meteorol.* **164**(2), 249–279 (2017).
24. P. J. Mason and S. H. Derbyshire, "Large eddy simulation of the stably-stratified atmospheric boundary layer," *Boundary-Layer Meteorol.* **53**, 117–162 (1990).
25. E. Saiki, C.-H. Moeng, and P. Sullivan, "Large-eddy simulation of the stably stratified planetary boundary layer," *Boundary-Layer Meteorol.* **95**, 1–30 (2000).
26. J. Kleissl, M. B. Parlange, and C. Meneveau, "Field experimental study of dynamic Smagorinsky models in the atmospheric surface layer," *J. Atmos. Sci.* **61**, 2296–2307 (2004).
27. E. Bou-Zeid, C. Higgins, H. Huwald, C. Meneveau, and M. B. Parlange, "Field study of the dynamics and modelling of subgrid-scale turbulence in a stable atmospheric surface layer over a glacier," *J. Fluid Mech.* **665**, 480–515 (2010).
28. T. Michioka, H. Takimoto, H. Ono, and A. Sato, "Reynolds-number dependence of gas dispersion over a wavy wall," *Boundary-Layer Meteorol.* **164**, 401–418 (2017).
29. M. R. Raupach, R. A. Antonia, and S. Rajagopalan, "Rough-wall turbulent boundary layers," *Appl. Mech. Rev.* **44**(1), 1–25 (1991).
30. C. L. V. Jayatilaka, "The influence of Prandtl number and surface roughness on the resistance of the laminar sublayer to momentum and heat transfer," *Progr. Heat Mass Transf.* **1**, 193 (1969).
31. C. Balaji, M. Hölling, and H. Herwig, "A temperature wall function for turbulent mixed convection from vertical, parallel plate channels," *Int. J. Therm. Sci.* **47**, 723–729 (2008).
32. T. Defraeye, B. Blocken, and J. Carmeliet, "CFD simulation of heat transfer at surfaces of bluff bodies in turbulent boundary layers: Evaluation of a forced-convective temperature wall function for mixed convection," *J. Wind Eng. Ind. Aerodyn.* **104**, 439–446 (2012).
33. V. B. L. Boppana, Z.-T. Xie, and I. P. Castro, "Thermal stratification effects on flow over a generic urban canopy," *Boundary-Layer Meteorol.* **153**, 141–162 (2014).
34. J. Fröhlich and D. von Terzi, "Hybrid LES/RANS methods for the simulation of turbulent flows," *Progr. Aerosp. Sci.* **44**, 349–377 (2008).
35. J. Thé and H. Yu, "A critical review on the simulations of wind turbine aerodynamics focusing on hybrid RANS-LES methods," *Energy* **138**(1), 257–289 (2017).
36. M. Shur, P. R. Spalart, M. Strelets, and A. A. Travin, "Rapid and accurate switch from RANS to LES in boundary layers using an overlap region," *Flow Turbul. Combust.* **86**(2), 179–206 (2011).
37. M. Labois and D. Lakehal, "Very-large eddy simulation (V-LES) of the flow across a tube bundle," *Nucl. Eng. Des.* **241**(6), 2075–2085 (2011).
38. C. Speziale, "Turbulence modeling for time-dependent RANS and VLES: a review," *AIAA J.* **36**(2), 173–184 (1998).
39. S. T. Johansen, J. Wu, and W. Shyy, "Filter-based unsteady RANS computations," *Int. J. Heat Fluid Flow* **25**(1), 10–21 (2004).
40. S. B. Pope, *Turbulent flows* (Cambridge University Press, Cambridge, 2000).
41. C. J. Greenshields, *OpenFOAM: The Open Source CFD Toolbox, User Guide, Version 4.0.* (OpenFOAM Foundation Ltd., London, 2016).
42. E. R. van Driest, "On turbulent flow near a wall," *J. Aeronaut. Sci.* **23**(11), 1007–1011 (1956).
43. M. Ricci, L. Patruno, and S. de Miranda, "Wind loads and structural response: Benchmarking LES on a low-rise building," *Eng. Struct.* **144**, 26–42 (2017).
44. Y. Ohya, "Wind-tunnel study of atmospheric stable boundary layers over a rough surface," *Boundary-Layer Meteorol.* **98**(1), 57–82 (2001).
45. B. Vreman, B. Geurts, and H. Kuerten, "Comparison of numerical schemes in large-eddy simulation of the temporal mixing layer," *Int. J. Numer. Meth. Fluids* **22**(4), 297–312 (1996).
46. P. Moin, "Advances in large eddy simulation methodology for complex flows," *Int. J. Heat Fluid Flow* **23**, 710–720 (2002).
47. P. Sagaut, *Large Eddy Simulation for Incompressible Flows: an Introduction* (Springer, Leipzig, 2006).

48. N. A. Adams, S. Hickel, T. Kempe, and J. A. Domaradzki, "On the relation between subgrid-scale modeling and numerical discretization in large-eddy simulation," in: *Complex Effects in Large Eddy Simulations*, Ed. by S. C. Kassinos, C. A. Langer, G. Iaccarino, and P. Moin (Springer, Berlin, 2007), pp. 15–27.
49. M. Kornhaas, D. C. Stenel, and M. Schafer, "Influence of time step size and convergence criteria on large eddy simulations with implicit time discretization," in: *Quality and Reliability of Large-Eddy Simulations*, Ed. by J. Meyers, B. J. Geurts, and P. Sagaut (Springer, Berlin, 2008), pp. 119–130.
50. D. Fauconnier, C. De Langhe, and E. Dick, "Construction of explicit and implicit dynamic finite difference schemes and application to the large-eddy simulation of the Taylor–Green vortex," *J. Comput. Phys.* **228**, 8053–8084 (2009).
51. M. Ahmadi-Baloutaki, R. Carriveau, and D. S.-K. Ting, "Effect of free-stream turbulence on flow characteristics over a transversely-grooved surface," *Exp. Therm. Fluid Sci.* **51**, 56–70 (2013).
52. J. C. Kaimal, J. C. Wyngaard, D. A. Haugen, O. R. Coté, Y. Izumi, S. J. Caughey, and C. J. Readings, "Turbulence structure in the convective boundary layer," *J. Atmos. Sci.* **33**, 2152–2169 (1976).